A HYBRID SOLAR IRRADIANCE NOWCASTING APPROACH: COMBINING ALL SKY IMAGER SYSTEMS AND PERSISTENCE IRRADIANCE MODELS FOR INCREASED ACCURACY

Bijan Nouri[1*], Niklas Blum[1], Stefan Wilbert[1], Luis F. Zarzalejo[2]
[1] DLR, Institute of Solar Research, Paseo de Almería 73-2, 04001 Almería, Spain
[2] CIEMAT Energy Department – Renewable Energy Division, Av. Complutense 40, 28040 Madrid, Spain

ABSTRACT: New technical challenges arise due to the growing share of distributed and intermittent solar power generation. Intra-minute and intra-hour variabilities, when insufficiently accounted for, could lead to grid instabilities. Shortest-term forecasts, often referred as nowcast, can anticipate such variabilities with high resolutions in space and time. Therefore, nowcasts are suited for fine-grained control applications in solar power plants and electrical grids. Highly resolve nowcasts can be obtained by all sky imager (ASI) systems. Sky conditions are analyzed and irradiance nowcasts a derived from the hemispherical sky images. In this work, ASI based nowcasts and persistence based nowcasts are combined to a hybrid nowcasts approach. This hybrid approach archived a reduction of the root mean square deviation of 12% over a 62-day lasting validation data set.

Keywords: Grid Integration, Grid Stability, Pyranometer, Solar Irradiance Nowcasts, All Sky Imager

1 AIM AND APPROACH USED

Reliable nowcasts of the solar irradiance become increasingly important, considering the rapid growth of solar power penetration. Applications include energy grid control [1] as well as ramp rate control within utility scale PV power plants [2]. Intra-hour and intra-minute variability of the incoming solar irradiance is mainly caused by clouds. Highly resolved observations of the sky can be obtained by all sky imagers (ASI), consisting of upward facing cameras with fisheye lenses. In recent years, methods have been developed to automatically detect clouds [3], evaluate the cloud radiative effect [4] and identify cloud motion vectors from such sky images [5]. If multiple cameras with overlapping viewing angles are available, cloud geolocalization can be performed using stereo photography [6]. A combination of such processing steps can be applied to derive irradiance nowcast [7]. Further methods of obtaining irradiance nowcasts are persistence approaches, which also serve regularly as control reference forecasting models. The performance of persistence approaches is often competitive in intra-hour nowcasting [8], considering the challenges of ASI based nowcasting systems [9]. This work presents a real time capable hybrid ASI and persistence nowcasting approach, which combines the strengths while reducing the respective weaknesses of both approaches.

2 SCIENTIFIC INNOVATION AND RELEVANCE

A nowcasting system based on two off-the-shelf Mobotix Q25 surveillance cameras has been developed at CIEMAT's Plataforma Solar de Almería (PSA). Hemispherical sky images with a resolution of 4.3 MP and an exposure time of 160 µs are taken every 30 s. The ASI nowcasting system also uses ground based irradiance measurements, taken directly next to one of the cameras. A detailed description of the used ASI system, with the already mentioned processing steps of cloud detection, evaluation of the radiative effect, tracking and geo-localization, is presented in [7]. The final output consists of global horizontal irradiance (GHI) maps, covering an area of up to 64 km² with a spatial resolution of 20 m and lead times up to 20 min ahead.

The utilized persistence nowcast is based on the work from Ineichen & Perez [10]. The prevailing Linke turbidity factor (TL) is calculated using the GHI measured by a pyranometer, h the height of the site, I0 the solar constant, r0 the average distance sun earth, r the current distance sun earth, α the solar altitude angle and AM the air mass.

$$TL = \left(\left(-1 \cdot \log\left(GHI/\left((5.09 \cdot 10^{-5} \cdot h + 0.868) \cdot I_0 \cdot (r_0/r)^2 \cdot \sin(\alpha)\right)\right) \cdot (1/(3.92 \cdot 10^{-5} \cdot h + 0.0387) \cdot AM)\right) - \exp\left(-\frac{h}{8000}\right)\right) \cdot 1/\exp\left(-\frac{h}{1250}\right) + 1 \qquad \text{Equation 1}$$

For the persistence nowcast, TL is kept constant while α and AM are calculated for the lead times > 0 min. Subsequently, the GHI persistence nowcast is calculated with the corresponding rearranged Equation 1.

A sliding validation of recent historical nowcast is performed between both nowcasting approaches and the ground based irradiance measurement. For this purpose, RMSD is calculated in real time according to Equation 2 using the pyranometer's GHI (GHI_{pyr}) of the past 5 minutes and the corresponding GHI nowcasts $GHI_{LT,j}$ for each delivered lead time. The index j indicates the two distinct nowcast approaches and the index LT the lead time. One RMSD is calculated for the ASI nowcast, another RMSD for the persistence nowcast. t_i describes the corresponding time stamp and n the selected time interval of 5 minutes.

$$RMSD_{LT,j} = \left[\frac{1}{n}\sum_{i=1}^{n}\left(GHI_{pyr}(t_i) - GHI_{LT,j}(t_i)\right)^2\right]^{0.5} \qquad \text{Equation 2}$$

Subsequently, current nowcasts $GHI_{LT,j}$ of both approaches for a given lead time are combined to the hybrid nowcast using the accuracy weighting approach described by [11] according to Equation 3.

$$GHI_{LT} = \frac{1}{\sum_{j=1}^{2}\frac{1}{RMSD_{LT,j}}} \cdot \sum_{j=1}^{2}\frac{GHI_{LT,j}}{RMSD_{LT,j}}$$

Equation 3

The ASI based, persistence based as well as the hybrid nowcasting approach are validated at PSA with 8 reference ground based stations distributed over an area of 1 km². The validation data set contains 62 variable days between 01.09.2019 and 30.11.2019. Figure 1 illustrates the GHI conditions within the validation data set.

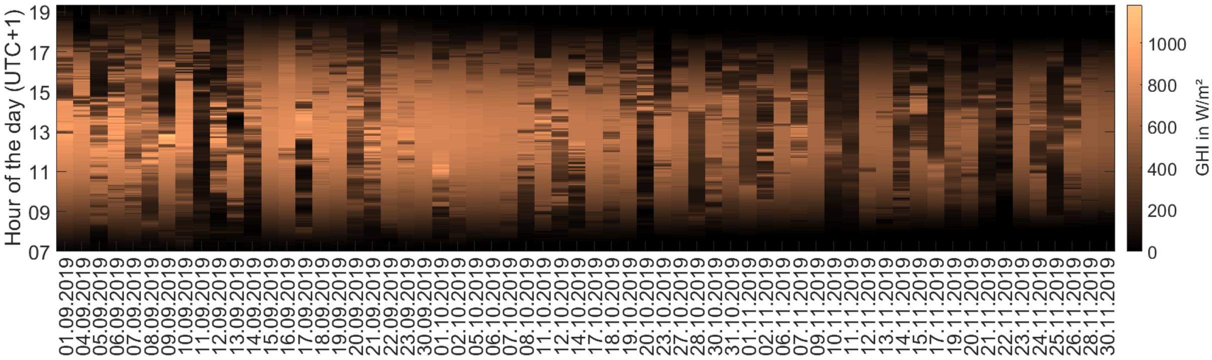

Figure 1: Overview of the validation data set containing 62 variable days between 01.09.2019 and 30.11.2019. The GHI corresponds to the arithmetic average of 8 reference pyranometers distributed over an area of 1 km².

The nowcasting accuracy strongly depends on the prevailing conditions. Comparatively high accuracy is reached during rather low variable conditions consisting of clear sky or overcast conditions. In contrast, lower nowcasting accuracies are reached during highly variable conditions, especially under conditions with fast moving low layer clouds or under complex multi-layer conditions. Overall, validation results for a given time interval without consideration of the prevailing conditions can lead to false impressions of the accuracy. Therefore, the validation data is discretized into eight distinct variability classes from clear sky (class 1) to overcast (class 8) according to [12]. Table I lists a short description of the variability classes.

Table I: Overview on used variability classes

Class	Sky conditions	Clear sky index	variability
1	Mostly clear sky	Very high clear sky index	Low variability
2	Almost clear sky	High clear sky index	Low variability
3	Almost clear sky	High/intermediate clear sky index	Intermediate variability
4	Partly cloudy	Intermediate clear sky index	High variability
5	Partly cloudy	Intermediate clear sky index	Intermediate variability
6	Partly cloudy	Intermediate/low clear sky index	High variability
7	Almost overcast	Low clear sky index	Intermediate variability
8	Mostly overcast	Very low clear sky index	Low variability

Figure 2 illustrates the distribution of the variability classes as well as the average GHI for each class within the validation data set. Around 57% of the data is comprised of the low variability conditions classes 1, 2 and 8. Intermediate and highly variable conditions comprise 34% and 9% of the data set, respectively. Most clear sky conditions at low solar altitude angles are classified in class 2, which results in comparably low GHI values within this class. The average GHI over the entire data set is 384 W/m². For the validation, RMSD is used as error metric, utilizing the entire data set discretized over the lead times. Furthermore, the validation is performed discretized over the lead times as well as the variability classes.

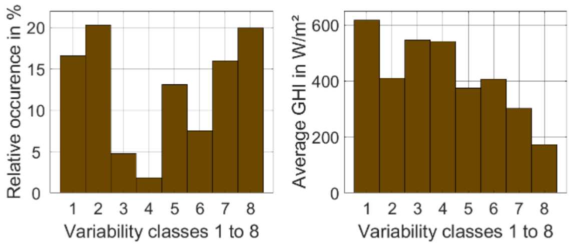

Figure 2: Distribution of the occurring variability classes (left) and average GHI within the classes (right) of the validation data sets.

3 RESULTS AND CONCLUSION

The overall validation results are shown in Figure 3. The ASI and persistence based nowcasts achieve similar RMSDs, with a slight advantage of the ASI based approach for the lead times 6 to 15 minutes ahead. In contrast, the hybrid nowcasting approach shows a significant performance improvement. An average reduction of around 12.6% in RMSD is visible over all lead times compared to the ASI or persistence based approach. Figure 4 shows the validation results discretized over the variability classes. Unsurprisingly, the lowest RMSD values are observed for the clear sky conditions class 1 and 2. Furthermore, as expected, the persistence approach shows an especially low RMSD for these low variable conditions. The third low variability condition class 8 (overcast) shows also low RMSDs. However, especially for the high lead times, the RMSDs are by a factor of up to three higher than for class 1 conditions. All three nowcasting approaches show similar RMSDs for class 8. For the intermediate variability condition class 3, the ASI based approach shows a significant advantage compared to the persistence approach. The remaining intermediate variability classes show similar performance of the ASI and persistence based nowcast, with a slight advantage for the persistence in class 5 and a slight advantage for the ASI in class 7. Both approaches are outperformed by the hybrid approach in all intermediate variability conditions. As expected, the persistence approach yields high RMSDs for the highly variable conditions classes 4 and 6. The ASI approach outperforms the persistence approach clearly in these cases, especially for class 4, whereas the ASI and hybrid approach show similar performances for both highly variable classes.

It was shown that ASI and persistence based nowcasting approaches show similar overall nowcast performances. However, clear differences are visible when discretizing the validation data in distinct variability conditions. As expected, persistence shows the best performance for low variability conditions, whereas it is outperformed by the ASIs during highly variable conditions. The clear division of strengths within distinct conditions is exploited by the hybrid approach, which clearly outperforms the ASI and persistence approach. The presented real time combination method is a promising approach to improve ASI based irradiance nowcasts.

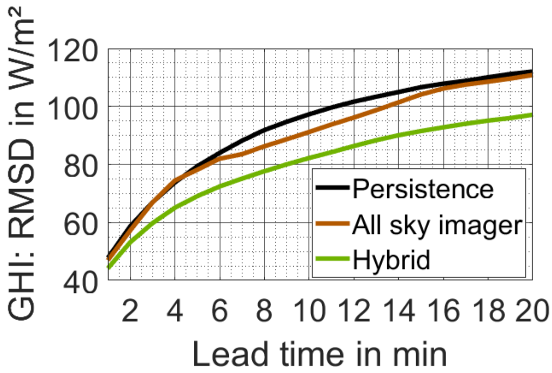

Figure 3: Overall RMSD over lead times of all three approaches.

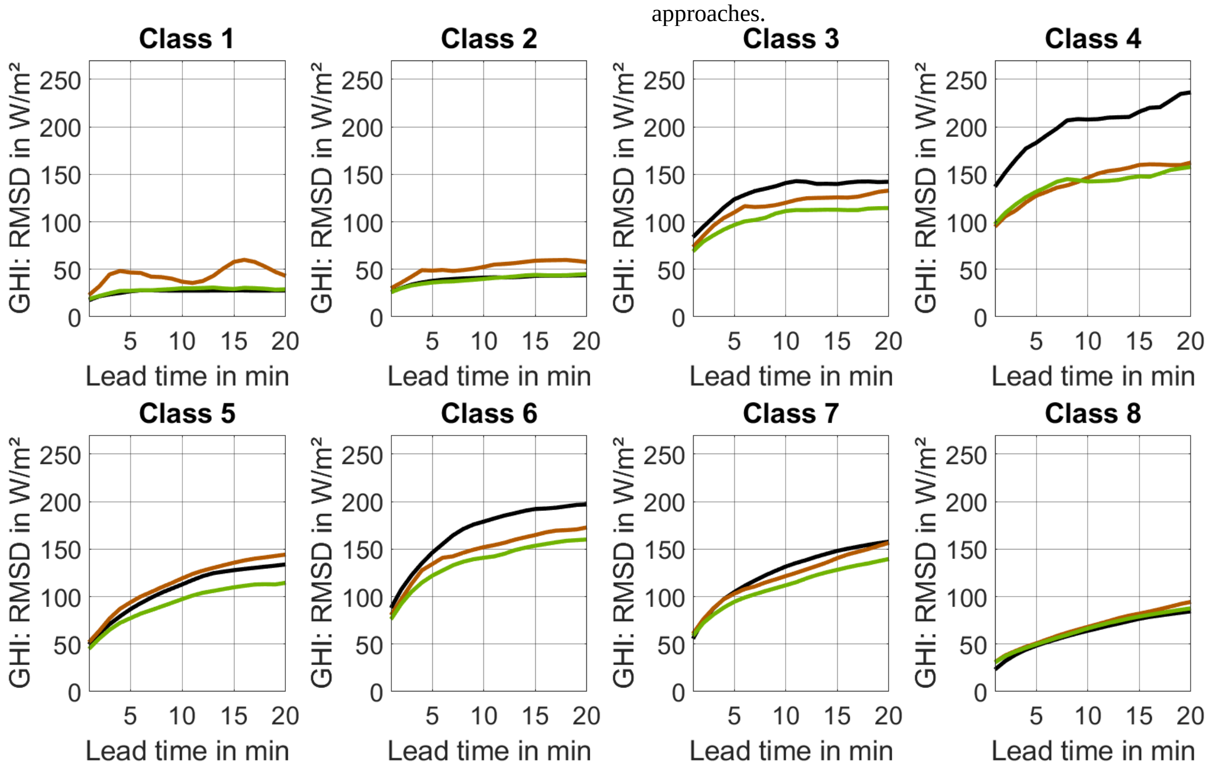

Figure 4: RMSD discretized over variability classes and lead times of all three approaches

ACKNOWLEDGEMENTS

This research received funding by the German Federal Ministry for Economic Affairs and Energy funded within the WobaS-A project (GrantAgreement no. 0324307A). Additional funding was received by the European Union within the H2020 program under the Grant Agreement no.864337 (Smart4RES).

REFERENCES

[1] Wan, C., Zhao, J., Song, Y., Xu, Z., Lin, J., & Hu, Z. (2015). Photovoltaic and solar power forecasting for smart grid energy management. *CSEE Journal of Power and Energy Systems*, *1*(4), 38-46.

[2] Cirés, E., Marcos, J., de la Parra, I., García, M., & Marroyo, L. (2019). The potential of forecasting in reducing the LCOE in PV plants under ramp-rate restrictions. *Energy*, *188*, 116053.

[3] Hasenbalg, M., Kuhn, P., Wilbert, S., Nouri, B., & Kazantzidis, A. (2020). Benchmarking of six cloud segmentation algorithms for ground-based all-sky imagers. Solar Energy, 201, 596-614.

[4] Tzoumanikas, P., Nikitidou, E., Bais, A.F., Kazantzidis, A., 2016. The effect of clouds on surface solar irradiance, based on data from an all-sky imaging system, Renew. Energy 95, 314–322.

[5] Peng, Z., Yu, D., Huang, D., Heiser, J., Yoo, S., Kalb, P., 2015. 3D cloud detection and tracking system for solar forecast using multiple sky imagers Sol. Energy 118, 496–519.

[6] Nguyen, D.A., Kleissl, J., 2014. Stereographic methods for cloud base height determination using two sky imagers. Solar Energy 107, 495–509.

[7] Nouri, B., Wilbert, S., Blum, N., Kuhn, P., Schmidt, T., Yasser, Z., ... & Pitz-Paal, R. (2020, December). Evaluation of an all sky imager

based nowcasting system for distinct conditions and five sites. In AIP Conference Proceedings (Vol. 2303, No. 1, p. 180006). AIP Publishing LLC.

[8] Kumler, A., Xie, Y., & Zhang, Y. (2018). A New Approach for Short-Term Solar Radiation Forecasting Using the Estimation of Cloud Fraction and Cloud Albedo (No. NREL/TP-5D00-72290). National Renewable Energy Lab.(NREL), Golden, CO (United States).

[9] Kuhn, P., Nouri, B., Wilbert, S., Prahl, C., Kozonek, N., Schmidt, T., Yasser, Z., Ramirez, L., Zarzalejo, L., Meyer, A., Vuilleumier, L., Heinemann, D., Blanc, P. and Pitz-Paal, R. Validation of an all-sky imager based nowcasting system for industrial PV plants, Prog Photovolt Res Appl., 1-14 (2017).

[10] Ineichen, P., Perez, R., 2002. A new airmass independent formulation for the Linke turbidity coefficient. Solar Energy 73, 151–157.

[11] Meyer, R., Geuder, N., Lorenz, E., Hammer, A., Ossietzky, C. Von, Oldenburg, U., Beyer, H.G., 2008. Combining solar irradiance measurements and various satellite-derived products to a site-specific best estimate, in: SolarPACES Conference. pp. 1–8

[12] Nouri, B., Wilbert, S., Kuhn, P., Hanrieder, N., Schroedter-Homscheidt, M., Kazantzidis, A., Zarzalejo, L., Blanc, P., Kumar, S., Goswami, N., Shankar, R., Affolter, R. and Pitz-Paal, R. Real-Time Uncertainty Specification of all Sky Imager Derived Irradiance Nowcasts. Remote Sens. 11(9), 1059 (2019).